1997 HST Calibration Workshop
Space Telescope Science Institute, 1997
S. Casertano, et al., eds.

STIS Observations of the Nuclear Ionized Gas in the Elliptical Galaxy M84

G. A. Bower[1], R. F. Green[1], D. Lindler[2], The STIS IDT

Abstract. We present optical long-slit spectroscopy of the nucleus of the nearby radio galaxy M84 (NGC 4374 = 3C 272.1) obtained with STIS aboard HST. Our spectra reveal that the nuclear gas disk seen in WFPC2 imaging by Bower et al. (1997, ApJ, 483, L33) is rotating rapidly. The velocity curve has an S-shape with a peak amplitude of 400 km s^{-1} at $0\farcs1 = 8$ pc from the nucleus. To model the observed gas kinematics, Bower et al. (1997, ApJL, in press) fit a thin Keplerian disk model to these data, leading to the conclusion that a $\approx 1.5 \times 10^9$ $M_\odot$ dark compact mass (most likely a supermassive black hole) resides in the nucleus of M84.

1. Introduction

M84 is an E1 galaxy in the Virgo Cluster with an active galactic nucleus and hosts the F-R I (Fanaroff & Riley 1974) radio source 3C 272.1. Bower et al. (1997a; hereafter Paper I) obtained images of M84 with WFPC2 aboard HST, showing that the ionized gas within the central kpc has three components: a nuclear gas disk, outer filaments, and an 'ionization cone'. The nuclear gas disk has diameter $\approx 1''$ (82 pc) and a major axis P.A. $\approx 58^\circ$ that is tilted by $\approx 25^\circ$ with respect to the major axis P.A. of the outer filamentary emission. This outer filamentary emission had been seen in ground-based imaging (e.g., Hansen et al. 1985; Baum et al. 1988). Its major axis is approximately perpendicular to the axis of the radio jets (Laing & Bridle 1987; Jones et al. 1981).

The presence of a nuclear gas disk in M84 is especially interesting. If the gas exhibits Keplerian motion about the nucleus, then a straightfoward application of Newton's laws to the dynamics of this gas disk would provide an estimate of the mass of the putative supermassive black hole (BH) in M84's nucleus. It is plausible that M84 contains a BH, since it is a radio galaxy and the rotation gradient of the ionized gas is spatially unresolved (i.e., > 100 km s^{-1} arcsec^{-1}) in ground-based observations (Baum et al. 1990, 1992). Previous HST observations using FOS have found gas-dynamical evidence for BHs in other galaxies containing nuclear gas disks, such as M87 and NGC 4261 (Harms et al. 1994; Ferrarese et al. 1996). STIS (through the use of a CCD in a long-slit spectrograph) provides a significant improvement in the HST efficiency for measuring the nuclear dynamics of galaxies. We chose M84 as a target for a demonstration.

2. Observations and Data Calibration

Long-slit spectroscopy of M84's nuclear region was obtained with the STIS CCD, which has a pixel scale of $0\farcs05$/pixel (Baum et al. 1996), aboard HST on 1997 April 14 and 17 with the telescope tracking in fine lock with one FGS probe (nominal jitter $\approx 0\farcs007$). Since M84's nucleus contains a bright optical point source (Paper I), the nucleus was acquired easily to

[1]NOAO/KPNO, P. O. Box 26732, Tucson, AZ 85726

[2]ACC, Inc., NASA/GSFC, Code 681, Greenbelt, MD 20771

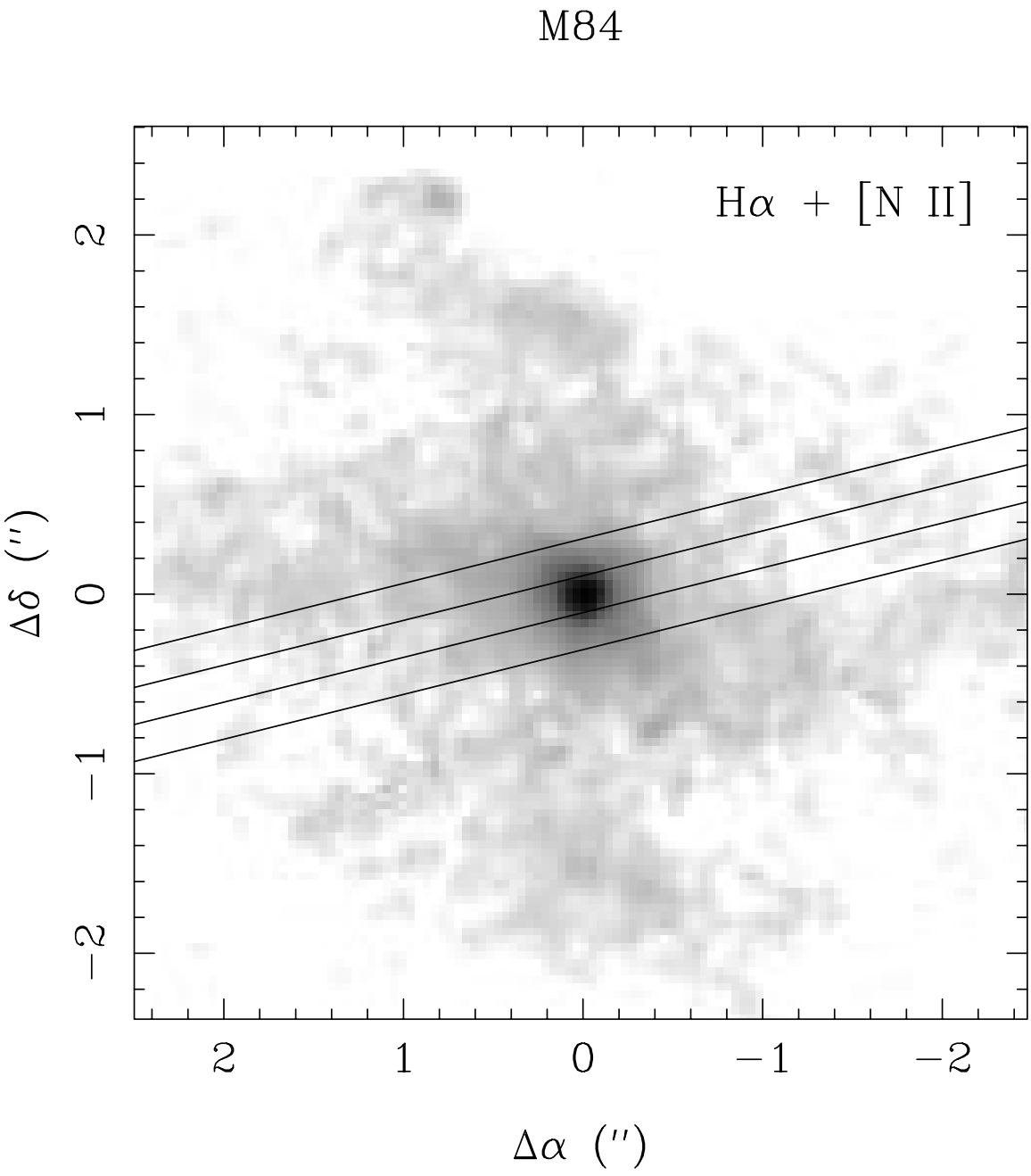

Figure 1. Our STIS slit positions (with the solid lines representing the slit edges) superposed on the Paper I Hα + [N II] image, which is displayed here with a logarithmic stretch with a range in intensity covering a factor of 100.

an accuracy of 0.″05 by the ACQ mode using two iterations of two 10 sec imaging exposures through the F28X50LP optical long-pass filter. The ACQ/PEAK mode (Baum et al. 1996) was not available during these observations since they were obtained early during Servicing Mission Orbital Verification (SMOV). The $52'' \times 0.''2$ slit was aligned at a position angle (P.A.) of 104°. This was the closest that the slit could be aligned with the gas disk's major axis (P.A. = 58°; Paper I) because of HST scheduling constraints during SMOV. To allow for the centering accuracy of only 0.″05 and for the offset between the slit P.A. and the gas disk's major axis, we planned to obtain spectra at four different slit positions offset from the nucleus by $-0.''3$, $-0.''1$, $+0.''1$, and $+0.''3$, where the offsets were perpendicular to the slit and negative spatial offsets moved the slit toward a P.A. of 14° on the sky. However, Bower et al. (1997b; hereafter Paper II) show that the actual offsets were $-0.''2$, $0.''0$, $+0.''2$, and $0.''0$ (see Fig. 1). For the fourth offset position, the discrepancy between the planned and actual positions occurred because this last spectrum was obtained during the second visit of M84, with an erroneously commanded offset. This error was fortuitous because from Paper II's analysis it is apparent that the kinematic signature of the nuclear gas disk is readily detectable only within $\sim 0.''3$ of the nucleus, beyond which the kinematics of the outer filamentary emission (which do not necessarily provide good leverage on the nuclear gravitational potential) dominates the spectrum.

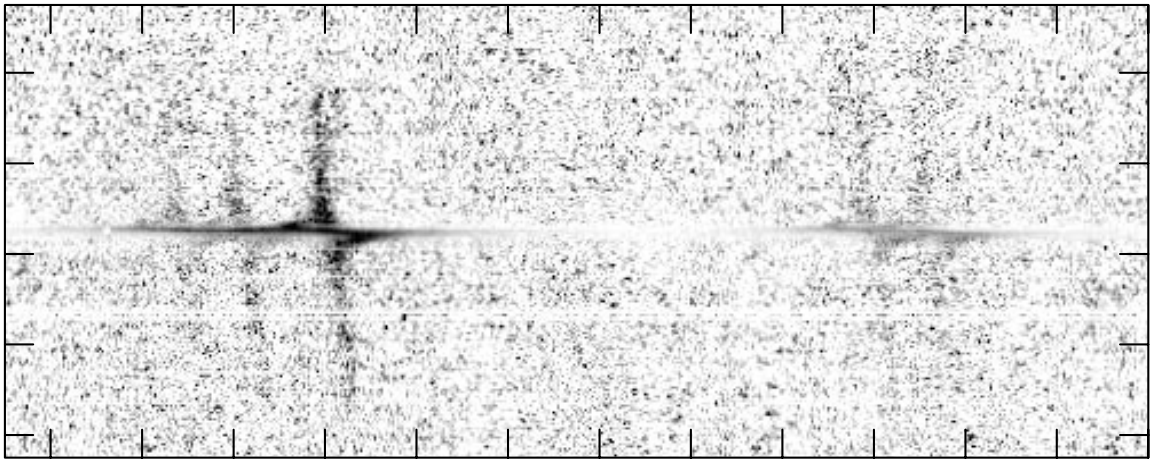

Figure 2. The central region of the last offset = 0.″0 spectrum, showing the emission lines (starting from the left) [N II] λ6548, Hα, [N II] λ6583, and [S II] $\lambda\lambda 6717, 6731$. To emphasize the velocity gradient, the continuum distribution has been subtracted, and each spectral row has been normalized by its peak intensity of the [N II] λ6583 line. The interval between tick marks is 40 pixels, which corresponds to 1000 km s^{-1} along the dispersion axis (horizontal), and 2″ along the spatial axis (vertical).

At each slit position, we obtained spectra with the G750M grating, which has a dispersion of 0.56 Å/pixel. This grating was set to cover the wavelength range of 6295 Å to 6867 Å, which includes the emission lines of Hα, [N II] $\lambda\lambda 6548, 6583$, and [S II] $\lambda\lambda 6717, 6731$. The spectral resolution of our instrumental configuration was 2.2 Å $\approx$ 100 km s^{-1} (FWHM), assuming uniform illumination of the slit. However, Paper I shows that at the nucleus, there is a point source in the optical continuum, and the Hα + [N II] emission is very compact. Thus, our spectral resolution at the nucleus was better than 100 km s^{-1}. We integrated for two HST orbits at each slit position, which was equivalent to $4500 - 5100$ sec per slit position depending on the occurrence of instrumental overheads. Spectra of the internal wavelength calibration source (wavecals) were interspersed among the galaxy spectra to allow for correction of thermal drifts during data reduction.

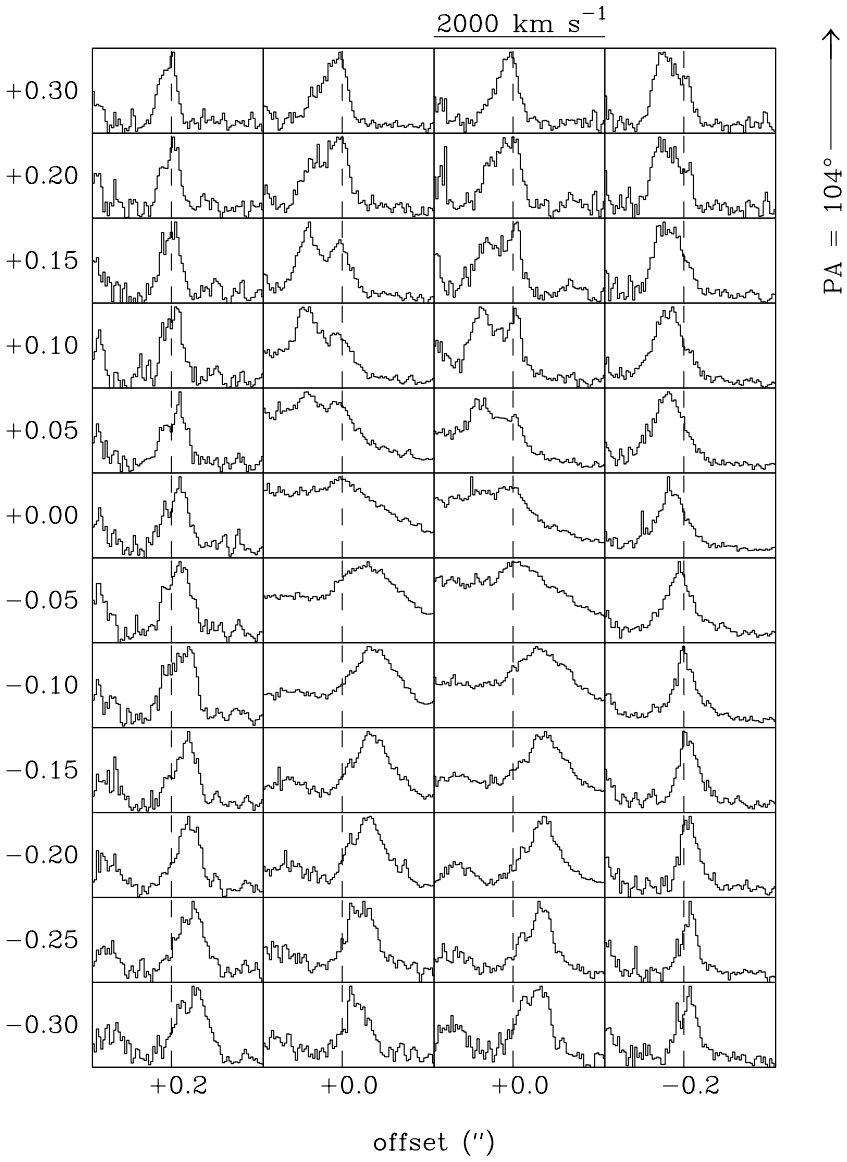

Figure 3. Profiles of the [N II] λ6583 emission line at positions within $\sim 0\farcs3$ of M84's nucleus. The spectra have been continuum subtracted and normalized to the peak intensity of [N II] λ6583. For each of the four slit positions, the offset from the nucleus is given along the bottom, where negative values of the offset move the slit toward P.A. = 14° on the sky. The position along the slit (relative to the nucleus) in arcseconds is shown on the left, where increasing values are toward P.A. = 104°. Each profile covers a heliocentric velocity range of $200-2200$ km s^{-1}, and the systemic velocity is indicated by a dashed line. All profiles were taken from a single row in the data, except for the profiles at $+0\farcs30$ along the slit which were binned by 4 pixels = $0\farcs2$ to improve the S/N.

The data were calibrated using the CALSTIS pipeline to perform the steps of bias subtraction, dark subtraction, applying the flatfield, and combining the two sub-exposures to reject cosmic-ray events. The accuracy of the flatfield calibration was 1%. To reject hot pixels from the data, we employed dark frames obtained immediately before and after the M84 observations. We examined the input data, the flagged hot pixels, and the cleaned output data to ensure that only hot pixels were rejected. The data were wavelength cali-

brated and rectified by tracing the wavecals (using the Ne emission lines for the dispersion axis and the shadows of the two occulting bars for the spatial axis) and then applying these solutions for the geometric distortions to the data. The largest offset that we found between the actual and nominal dispersion solutions was 0.30 pixels, which is significant given that the dispersion solutions were accurate to 0.06 pixels (0.03 Å = 1 km s^{-1}). The data were then rebinned onto a log λ scale with a reciprocal dispersion of 25 km s^{-1} $pixel^{-1}$.

3. Measurement of the Gas Kinematics

The first iteration at measuring the radial velocities involved cross correlating each spectral row from the four long-slit spectra with a synthetic emission-line spectrum, which included only the five emission lines that we detected in M84 (see Fig. 2) with flux ratios set at values typically found in the data. We then compared the velocities measured by the cross correlation technique with those measured manually from the emission-line peaks. These measurements agree very well for distances $> 0\farcs3$ from the nucleus. For rows closer to the nucleus than this, the emission line profiles usually exhibit two kinematic components rather than a single component. These two components are readily seen in the strong [N II] λ6583 profile (as shown in Fig. 3), especially for the two spectra with offset = $0\farcs0$. Since the velocity measured by our cross correlation technique (using our synthetic template spectrum) coincides with the flux-weighted centroid over a given emission-line profile, these measurements will be distorted when more than one kinematic component is present. We determined which of the [N II] λ6583 profiles in Fig. 3 have two kinematic components by fitting model profiles to a few examples. Separate models with one or two Gaussians were fit to the profiles. If the improvement in χ^2 was significant, then the profile was classified as having two kinematic components. Although these models were not good fits to the observed profiles (which have broader wings than a Gaussian), this procedure was sufficient for objectively determining which profiles have two components. The velocities for the separate components were then measured by finding the centroid of each component peak.

Based on the Hα + [N II] image (see Fig. 1), it is not surprising that two kinematic components are seen within $\sim 0\farcs3$ of the nucleus in the STIS spectroscopy. Paper I identified three spatial components in the ionized gas, including the nuclear gas disk, the outer filaments, and an ionization cone. Given these spatial components, the line of sight to the nuclear gas disk should also intersect the outer filamentary gas (and perhaps the ionization cone) lying in the foreground. Since the outer filamentary gas rotates about the nucleus at $\approx \pm 100$ km s^{-1} (Baum et al. 1990, 1992), one expects to see this low-velocity component superposed onto the high-velocity kinematics of the nuclear gas disk. Fig. 4 shows our velocity measurements along the slit for each of the four slits. Our measurements of the low-velocity component agree very well with those of Baum et al. (1990). This measurement of the high-velocity component is the first time that the kinematics of M84's nuclear gas disk have been resolved. Paper II analyzes these data in more detail, leading to the conclusion that a $\approx 1.5 \times 10^9$ $M_\odot$ dark compact mass (most likely a supermassive black hole) resides in the nucleus of M84.

Acknowledgments. We acknowledge useful discussions with Eric Emsellem and Ralf Bender as well as the assistance of Pat Hall and Charles Liu in planning these observations. Support for this work was provided to the STIS Investigation Definition Team by NASA.

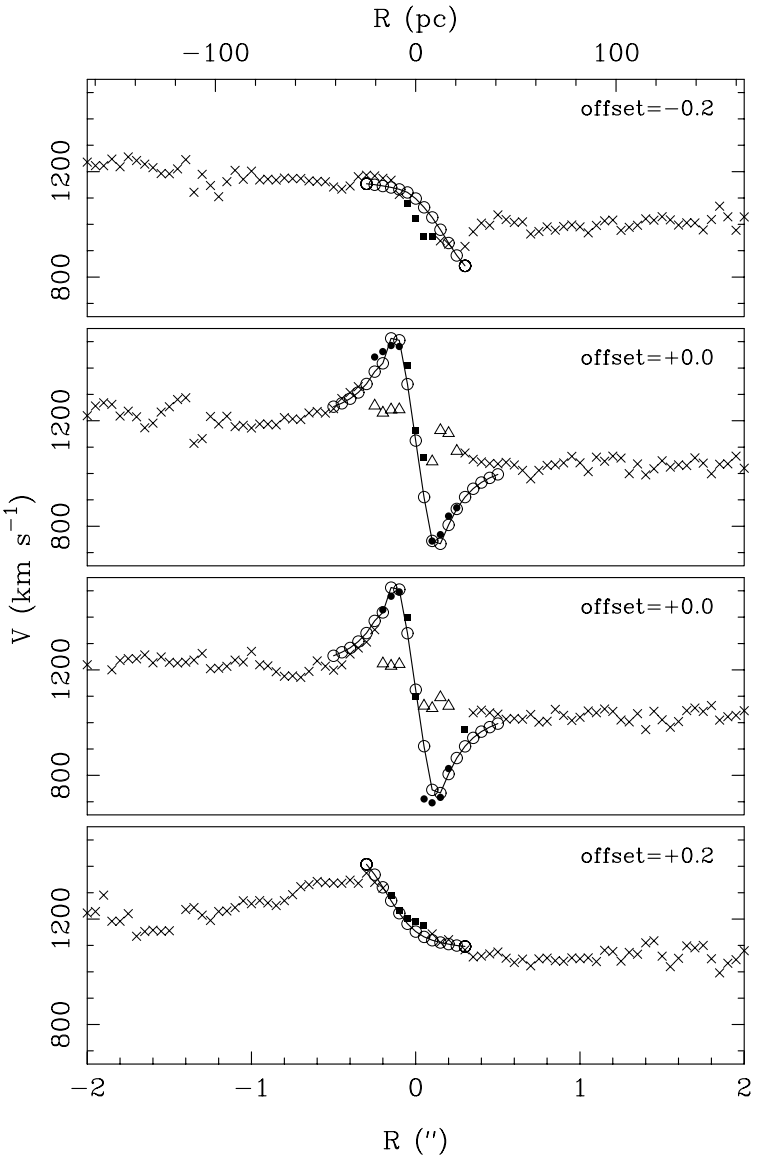

Figure 4. The heliocentric velocity as a function of distance along the slit for each slit position. Crosses indicate velocities measured by the cross correlation technique described in the text. Closer to the nucleus where two kinematic components are present, open triangles represent the low-velocity component, and filled circles or squares represent the high-velocity component. The squares denote positions where the high-velocity and low-velocity components cannot be separated because both are at or near the systemic velocity. The errors in the data points are ≤ 25 km s^{-1} (i.e., no larger than the size of the points). The velocities predicted by the best fit thin Keplerian disk model are represented by open circles connected by a solid line.

References

Baum, S., et al. 1996, *STIS Instrument Handbook* Version 1.0 (Baltimore: STScI)
Baum, S. A., et al. 1988, ApJS, 68, 643
Baum, S. A., Heckman, T., & van Breugel, W. 1990, ApJS, 74, 389
Baum, S. A., Heckman, T., & van Breugel, W. 1992, ApJ, 389, 208
Bower, G. A., Heckman, T. M., Wilson, A. S., & Richstone, D. O. 1997a, ApJ, 483, L33 (Paper I)
Bower, G. A., Green, R. F., et al. 1997b, ApJL, in press (Paper II)
Fanaroff, B. L., & Riley, J. M. 1974, MNRAS, 167, 31P
Ferrarese, L., Ford, H. C., & Jaffe, W. 1996, ApJ, 470, 444
Hansen, L., Nørgaard-Nielsen, H. U., & Jørgensen, H. E. 1985, A&A, 149, 442
Harms, R. J., et al. 1994, ApJ, 435, L35
Jones, D. L., Sramek, R. A., & Terzian, Y. 1981, ApJ, 246, 28
Laing, R. A., & Bridle, A. H. 1987, MNRAS, 228, 557